Robust Quantification of the Burst of OH Radicals Generated by Ambient Particles in Nascent Cloud Droplets using a Direct-toReagent Approach

5

Sina Taghvaee^{§,a}, Jiaqi Shen[§], Catherine Banach, Chris La^b, Steven J. Campbell^c, and Suzanne E. Paulson*

9

Department of Atmospheric & Oceanic Sciences, University of California, Los Angeles, CA 90095, USA

12

13

- 1415 §Co-first author
- *Corresponding author:
- 17 Professor Suzanne E. Paulson
- 18 Chair, Department of Atmospheric and Oceanic Sciences
- 19 7127 UCLA Math Science building, Los Angeles, CA 90095
- 20 E-mail: Paulson@atoms.ucla.edu
- 21 Telephone: 310 206 4442

22 23

^aNow at: Planning, Rule Development and Implementation Division, South Coast Air Quality Management District, 21865 Copley Dr, Diamond Bar, CA 91765

242526

^bNow at: Department of Chemistry, University of California Berkeley, Berkeley, CA 94720

27 28

^cNow at: MRC Centre for Environment and Health, Environmental Research Group, Imperial College London, 86 Wood Lane, London W12 oBZ, UK.

30

29

31

Abstract

33

Reactive oxygen species (ROS) play a central role in chemistry in cloud water, as well as in 34 other aqueous phases such as lung fluid and in wastewater treatment. Recently work 35 simulating nascent cloud droplets showed that aerosol particles produce a large burst of 36 OH radicals when they first take up water. This activity stops abruptly, within two minutes. 37 The source of the OH radicals is not well understood, but it likely includes the aqueous 38 phase chemistry of ROS and/or organic hydroperoxides and redox active metals such as 39 iron and copper. ROS and their precursors are in general highly reactive and labile, and 40 thus may not survive during traditional sampling methods, which typically involve multi-41 hour collection on a filter or direct sampling into water or another collection liquid. 42 Further, these species may further decay during storage. Here, we develop a technique to 43 grow aerosol particles into small droplets and capture the droplets directly into a vial 44 containing the terephthalate probe in water, which immediately scavenges OH radicals 45 produced by aerosol particles. The method uses a Liquid Spot Sampler. Extensive 46 characterization of the approach reveals that the collection liquid picks up substantial 47 OH/OH precursors from the gas phase. This issue is effectively addressed by adding an 48 activated carbon denuder. We then compared OH formation measured with the direct-to-49 reagent approach vs. filter collection. We find that after a modest correction for OH formed 50 in the collection liquid, the samples collected into the reagent produce about six times 51 those collected on filters, for both PM_{2.5} and total suspended particulate. This highlights 52 the need for direct-to-reagent measurement approaches to accurately quantify OH 53 production from ambient aerosol particles. 54

Key words

56 Liquid spot sampler, OH burst, online aerosol measurement, cloud chemistry

57

58

59

60

61

62

63

64

65

66

67

68

69

70

71

72

73

55

1. Introduction

Atmospheric aerosols have widespread impacts on ambient air quality, health, the climate system, and radiative forcing. Hydroxyl radical-driven aqueous-phase atmospheric chemistry in clouds is a potentially important pathway leading to the formation of secondary organic aerosol, which constitutes a substantial fraction of ambient particles (Ervens et al. 2014, El-Sayed et al. 2015, Sareen et al. 2016). Cloud-water chemistry, such as aqueous phase reactions of phenolic compounds, is also recognized as a major contributor to the formation of extremely low-volatility organic compounds (Yu et al. 2016). In addition, while the first step in dimethyl sulfide oxidation takes place mostly in the gas phase, efficient oxidation of the intermediate oxidation products such as methane sulfonic acid and dimethyl sulfoxide (DMS), depends on the aqueous phase chemistry of cloud and fog droplets (Hoffmann et al. 2016). DMS oxidation is estimated to contribute more than 18% of sulfate global direct radiative forcing and more than 50% of the global incremental indirect radiative forcing, and in parts of the pristine atmosphere this is very sensitive to OH_{ao}-driven aqueous cloud chemistry (Bardouki et al. 2002, Yang et al. 2017, Fung et al. 2022).

To investigate the rate of OH formation in cloud droplets, researchers have exposed authentic cloud water samples to sunlight in the laboratory (Arakaki and Faust 1998, Bianco et al. 2015, Kaur and Anastasio 2017). Results of these studies revealed a significantly lower OH production rate (i.e., $(0.003 - 0.3) \times 10^{-9} \text{ M s}^{-1}$) compared to the direct uptake rate of gas-phase OH radicals of about 2×10^{-9} M s⁻¹ (Hanson et al. 1992, Arakaki and Faust 1998, Bianco et al. 2017). The sources of the slow formation of OH in cloud droplets include: the Fenton reaction (Zepp et al. 1992), the 'photo-Fenton' reaction, in which Fe (III) is photoreduced to Fe (II), followed by the Fenton reaction (Zepp et al. 1992, Nguyen et al. 2013), the reaction of superoxide with ozone, and the direct photolysis of various compounds including H2O2 (Zellner et al. 1990), iron hydroxides (Deguillaume et al. 2005), nitrate and nitrite ions (Ervens et al. 2014). At higher pHs (> 6), the reaction of O_3 with O_2 may also contribute (Sehested et al. 1983). However, due to evidence of rapid consumption of OH in droplets (Luo et al. 2017), aqueous OH is believed to be strongly undersaturated (Ervens 2018). The above sources are not sufficient to explain the oxygen-to-carbon (O/C) ratios observed in cloud water (Ervens et al. 2014), indicating a missing source(s) of OH radicals.

Recently, Paulson et al. (2019) found that simulating cloud droplet chemistry by adding water to ambient particles collected on filters and illuminating the resulting solutions led to a burst of OH radical formation. They observed an OH formation at a rate of $\sim 1-30 \times 10^{-9}$ M s⁻¹ lasting for about two minutes and stopping abruptly. These OH_{aq} formation rates range from about equal tomuch larger than gas-phase uptake (above). Since cloud droplet lifetimes are generally fairly short, on the order of 10 minutes, the burst of OH formation should be a substantial or dominant source of OH radicals in the droplets.

74

75

76

77

78

79

80

81

82

83

84

85

86

87

88

89

90

91

92

93

94

Growing evidence indicates many ROS are short lived, decaying rapidly after generation both in the atmosphere and when the particles are collected on filters, with half-lives as low as several minutes (Fuller et al. 2014, Bates et al. 2019, Zhang et al. 2022). The atmospheric lifetime of organic peroxides, important OH_{aq} precursors, varies from ~seconds to several days, depending on the loss pathway and organic peroxide structure (Wang et al. 2023). Consequently, the quantification of OH_{aq} by collecting particles on filters for many hours followed by aqueous extraction may obscure rapid chemistry that takes place as cloud droplets form, underestimating the true extent of OH formation and emphasizing the need for the rapid collection of particles to capture the chemistry of highly reactive aerosol components.

To avoid the abovementioned issues and better simulate processes taking place in clouds, we developed a method to measure OH formation by the particles once they are dissolved in water as in cloud droplets. For this 'Direct-to-Reagent' (DtR) approach, the ambient particles are grown to be small droplets and are then captured within 0.3 s directly into acidic water containing an OH probe, present in excess. The collection system uses a Liquid Spot Sampler (Aerosol Devices Inc.). Because the collection liquid is also exposed to the gas phase, we thoroughly characterized the uptake of OHg and OH precursors from the gas phase, such as OHg, volatile organic compounds, H₂O₂, and O₃. Because this source of background OHaq was significant, we devised a method to remove gas phase species which may complicate particle-generated OHaq quantification.. Next, we explore the relationship between the OH burst measured with DtR and filter sampling, and how this relationship

changes with particle size. As far as we are aware this is the first direct measurement of OH formation by aerosols sampled directly into a reagent solution.

2. Methods

2.1 Materials and Trace Metal Cleaning

Disodium terephthalate, and 2-hydroxyterephthalic acid were purchased from TCI America (Portland, OR, USA). 2,2,2-Trifluoroethanol, ammonium sulfate crystals, and 0.1 N sulfuric were purchased from Sigma-Aldrich. Nitric acid (70% trace metal grade) was purchased from Fisher Scientific (Pittsburg, PA, USA). Ethanol (200 proof) was purchased from Decon Labs.

A rigorous cleaning process including acid soaking and multiple rinses was followed for all glass and Teflon containers, as detailed in Kuang et al. (2017). 18.2 M Ω cm $^{-1}$ MilliQ water was used for cleaning and to prepare reagent solutions. pH was measured with a bench top pH meter (HANNA instruments, HI 3220), calibrated daily with pH 4, 7, and 10 standards.

2.2 Quantification of Hydroxyl Radical Formation and Particle Mass

The terephthalate (TA) probe was used to quantify OH concentrations. Excess terephthalate (10 mM) scavenges OH, and reacts to form a strongly fluorescent product, 2-hydroxyterephthalic acid (hTA), with 31.5% yield at pH 3.5 and 31.9% at pH 4.5 (Gonzalez

et al. 2018), the pHs of our collection solutions. hTA was detected at $\lambda_{ex}/\lambda_{em}$ of 320/420 nm (with 10 nm slit width at half maximum) with a fluorometer (Lumina, Thermo Scientific). The fluorometer exposes the samples to 9 s of light, makes a 10 ms fluorescence measurement, and repeats this twice more in succession. Calibration curves were constructed daily for the appropriate conc. range depending on the measurement that day, usually 0.25 - 3 \times 10⁻⁷ M hTA. More details regarding the cumulative OH_{aq} formation quantification can be found in Kuang et al. (2020).

Particle mass loadings on collected filters were determined gravimetrically with a microbalance (1 μ g precision, ME 5, Sartorius) after charge neutralizing with a ²¹⁰Po neutralizer (Model 2U500, NRD Inc., USA).

2.3 Direct - to - Reagent OH (DtR) Sampling

Particles were collected at a flow rate of 1.5 LPM, grown into small droplets, and deposited into the liquid containing the OH probe by using a Series 110A-BC Spot Sampler aerosol particle collector (Aerosol Devices Inc., USA). The spot sampler collects more than 90% of total suspended particulate (TSP) > 5 nm. Previous studies have documented the robust collection of PM-bound volatile constituents as well as excellent conservation of ambient aerosol chemical composition with this aerosol into liquid collector technology (Hecobian et al. 2016, Eiguren-Fernandez et al. 2017, Kunihisa et al. 2020).

In summary, the spot sampler grows incoming particles by condensing water vapor on aerosols to form microdroplets using a three-stage laminar flow growth tube lined with

a wetted wick that creates water vapor saturation (Fig. 1 left panel): (i) The 1st stage is a conditioner that provides a cool environment (around 5 °C) to establish a controlled saturated aerosol stream. (ii) The incoming particles then travel to the second stage which has a wetted wall that is set about 35 °C higher than the first stage. The higher diffusive rate of water vapor compared to the thermal diffusivity of air (and therefore heat transfer from the wall) forces the additional water vapor to diffuse into the flow stream, creating a supersaturated environment. In this stage, particles as small as 5 nm act as condensation nuclei and grow into ~3 µm droplets. The incoming flow should at most reach temperatures slightly higher than ambient (i.e., less than 3 °C, Hering et al. (2014)), minimizing potential artifacts from reactions or processes facilitated by elevated temperatures. (iii) Finally, the third stage consists of a cooled moderator with a wall temperature set to 18-20°C. This allows continued droplet growth at near ambient temperatures, while reducing the flow temperature and water vapor content. The grown particles (containing water) are then collected at the base of the growth tube in a polycarbonate vial containing water with the OH probe. The whole process from the beginning of water uptake to collection in the sample vial takes 0.33 seconds.

Cleaning the sample collection vial and several of the Spot Sampler components is essential to produce reliable data. Our cleaning protocol became more involved as the study progressed, which likely had some impact on the data presented, in particular causing intercepts for the data collected without the denuder; see below. The final cleaning protocol consists of: (1) injecting 500 counts of ethanol followed by 1000 counts of water at the end of each sampling period to clean the flow tube; and (2), overnight soaking of the

158

159

160

161

162

163

164

165

166

167

168

169

170

171

172

173

174

175

176

177

178

collection vial in 2% nitric acid prior to the next sampling followed by multiple rinses and (3) regular careful cleaning of the nozzle that directs the sample flow to the collection vial.

2.3.1 Direct to Reagent Sampling Setup

The collection liquid contained a 10 mM solution of aqueous the TA probe adjusted to pH 3.5 (Los Angeles data) or 4.5 (Oklahoma data) with 0.1 N sulfuric acid. In all cases, the collection vial was filled with 550 µl of the TA solution at the beginning of each sample collection, and the volume was maintained between 450 and 550 µl during sampling. These vial volumes are kept within this range to ensure efficient droplet collection in the Spot Sampler.

To size select PM_{2.5}, a Sioutas Personal Cascade Impactor (PCIS, SKC Inc., USA) (Misra et al. 2002) was attached upstream of the PM spot sampler. Since the nominal working flowrate of the PCIS is 9 LPM, a portable vacuum pump (Leland, SKC Inc., USA) was run in parallel with the spot sampler to provide a bypass flowrate of 7.5 LPM. We used the PCIS with only stage A installed to capture PM_{2.5}.

2.3.2 Characterization of the Gas Phase Uptake of OH/OH precursors Associated with Direct-to-Reagent Sampling.

There are two potential pathways by which gas-phase OH (OH_g) or OH precursors might be taken up during sampling. Gases can be incorporated into the nascent droplets as they form in the growth tube (Figure 1) or they can be taken up directly by the reagent

solution as the sample flow passes over the surface of the collection liquid. We used several different configurations to test the full background of the spot sampler and its potential uptake of ambient gas-phase hydroxyl radicals (OH_g) and other gases that can lead to formation of OH_{aq} in the collection liquid.

In config. 1, we introduced compressed air (presumably containing negligible OH_g) (Medical air USP grade including 76.5 - 80.5% N_2 and 19.5-23.5% O_2) from a cylinder (Airgas Inc.) at a flowrate of 1.5 LPM into the spot sampler (SI Figure S1(a)). In config. 2, laboratory generated ammonium sulfate aerosols were added to the cylinder air flow (SI Figure S1(b)). $(NH_4)_2SO_4$ particles were generated with a commercially available B&B HOPE atomizer (Model 11310, USA), and cylinder air (at 1.34 atmosphere) into the atomizer to nebulize 16 μ g/ml aqueous $(NH_4)_2SO_4$ into small droplets. A DiSCMini (Testo, Switzerland) which measures particle number in the 10 – 700 nm range monitored the number concentration of the aerosolized ammonium sulfate prior to their collection in the Spot Sampler. The measured particle number concentration was 9.87×10^5 cm⁻³ and median diameter was 500 nm.

Configs. 3 -5 were designed to quantify uptake of OH_g or its precursors from the gas phase: In config. 3, a HEPA-vent filter (Whatman 6723-5000, UK) upstream of the spot sampler removed particles to probe the uptake of OH_g and OH precursors from the gas phase (SI Fig. S1(c)). In config. 4, we added laboratory-generated (NH₄)₂SO₄ to the PM-filtered ambient air in config. 3 (SI Fig. S1(d)). Finally, in config. 5, the ambient air passed through a HEPA-vent filter and a honeycomb activated carbon gas denuder (Aerodyne Research, Inc., USA) upstream of the spot sampler to remove both particles and gases from the air

stream (SI Figure S1(e)). The denuder has been reported to remove > 99.9% of organic gases at flow rates < 2 LPM, as well as efficiently removing O_3 without major impacts on relative humidity (Campbell et al. 2019) and with only a small amount of particle loss. We also measured particle loss for ambient air with a DiSCMini using a parallel configuration with and without the denuder.

2.4 Ambient Sample Collection and Extraction

Ambient gas and aerosol samples were collected on the rooftop of the UCLA Mathematical Sciences Building (34°04′10.1″ N, 118°26′35.3″ W, 32 m above ground level), located near western Los Angeles edge of the area, ~8 km from the Pacific Coast. Additional tests of the gas phase denuder were performed at the Department of Energy Southern Great Plains Site located in Tonkawa, Oklahoma (36°36′27.6″N 97°29′25.4″W), 2 m above ground level.

For filter and direct-to-reagent (Spot Sampler) collection comparisons, particles were collected in parallel on acid washed 47mm-Teflon filters (PALL corporation, USA, 2 µm pore size) and with the Spot Sampler at the UCLA site for ~4-7 hours, starting from about 10:00 am on 12 days during April and Aug. – Nov., 2021, divided into 8 and 9 PM_{2.5} and TSP samples, respectively. A cyclone inlet (URG corporation, USA, Model 2000-30E-42-2.5 or 2000-30EP) was used to collect ambient PM_{2.5} and on filters at a flowrate of 92 LPM (SI Figure S2). Total suspended particulate (TSP) was collected directly onto a filter at 90 LPM with a BGI aluminum filter holder with its cover attached (Mesa Labs Inc., USA).

Filters were pre- and post-weighed using a microbalance (Sartorius ME-5) to calculate the collected particulate mass. Blank filters were created in the same way as samples but with the vacuum pump turned on for only 30 seconds. Filter samples were frozen until analysis and were analyzed within 3 days.

All reported aerosol data have been normalized to an aerosol:water volume ratio (i.e., aerosol volume/extraction solution volume) of 25,000 (typical of cloud water) assuming an aerosol particle density of 1.2 g cm⁻³ (Hasheminassab et al. 2014); Spot Sampler samples are much more dilute, with aerosol:water v:v ratios that were in the range (1.4 × $10^4 - 1.6 \times 10^5$). The extraction volume for filter samples was adjusted according to collected aerosol particle mass (obtained with a microbalance, Sartorius) to give the desired 25,000 v:v ratio (Kuang et al. 2020). Filter samples were wetted with 50 μ L of 2,2,2-trifluoroethanol (TFE), and then extracted in aqueous pH 3.5 solution containing 10 mM of TA with gentle agitation at 20 rpm on a shaker (Heidolph, Rotomax 120) in the dark.

2.5 Background and Blank OH Corrections for Filter and Direct-to-Reagent Samples

The ambient filter samples were corrected with blank filters. Blanks for different configurations of DtR samples are summarized in Table 1 (config. 1-5). Ambient PM samples collected without a denuder (config. 6, collected during daytime), were blank corrected by multiplying the sampling time by the average OH_{aq} formation rate for all daytime PM-filtered ambient air samples collected without a denuder (config. 3). The ambient samples

collected with a denuder (config. 7) were corrected with the OH_{aq} formation for the PM-filtered ambient air with a denuder (config. 5), a much smaller correction.

In previous work on ambient samples, slow formation of OH was observed in the filter extracts (Paulson et al. 2019, Kuang et al. 2020), consistent with the OH sources other than the burst (see Introduction). It is reasonable to assume this chemistry also takes place in the collection liquid during multi-hour collections with the Spot Sampler. To correct for this, we subtracted the slow OH formation observed in filter samples collected in parallel, for a length of time equal to ½ of the sample collection period.

3. Results

3.1. OH_{aq} in the Collection Liquid from the Gas Phase

OH_g and OH precursors may be captured from ambient air flowing over the surface of the reagent solution or may be taken up by droplets created in the growth tube and deposited into the solution. The latter scenario does take place during droplet formation in the atmosphere, but because the droplets in our system are captured within a fraction of second and are not grown at the same rates as real cloud droplets, we cannot accurately simulate gas phase uptake by cloud droplets. Either scenario interferes with OH_{aq} measurements from particles themselves, the focus of this study. Figure 2 shows the results of tests of six types of air without ambient particles, testing one or both of these pathways. The tests used cylinder, PM-filtered nighttime or daytime air with or without aerosolized $(NH_4)_2SO_4$, as well as gas denuded, PM-filtered ambient air (Table 1).

After subtraction of the TA solution background, the cylinder air with and without aerosolized (NH₄)₂SO₄ and nighttime PM-filtered air resulted in consistently low OH_{aq} concentrations (21 - 31 nM) independent of the collection period (Configs. 1 - 3, Table 1). We believe trace contaminants in the vial, the nozzle and other trace contaminants that can accumulate in the instrument (see methods) resulted in this "intercept". With our improved cleaning protocol this "intercept" has essentially disappeared, leading to a lower and more consistent background, and allowing for more accurate quantification of OH_{aq}.

Gas phase-only samples collected during daytime (configs. 3 and 5) are plotted as a function of sampling time (Fig. 2), and of time of day (Fig. 3). Each point (Fig. 2) or line (Fig. 3) was collected on a different day; for the UCLA samples, meteorology was similar from day to day. Uptake of OH_g from the gas phase clearly increased with sampling time, linearly within error, with some day-to-day variation. Day time gas phase-only samples collected without a denuder had an average slope of 32 ± 4 nM/hr (Fig. 2 blue circles and Fig. 3 black lines). Since particles had been removed using a HEPA filter, the OH_{aq} signal is from uptake from the gas passing over the collection liquid in the vial. 32 nM/hour is equivalent to an ambient concentration of about 1.2 × 108 molec/cm3, well above the expected OH_g concentration in Los Angeles in the late spring/summer/fall mid-day when the measurements were made. Reported daytime OH_g concentrations at a site about 30 km inland from ours in 2010 averaged $\sim 4 \times 10^6$ molec/cm³ with a maximum at $\sim 8 \times 10^6$ molec/cm³ (Griffith et al. 2016). Further, measured OH_g values have rarely exceeded ~10⁷ molec/cm3 in any field campaign anywhere around the globe. are responsible for the elevated background signal. The existing gas phase background signal implies that the

284

285

286

287

288

289

290

291

292

293

294

295

296

297

298

299

300

301

302

303

304

collection liquid is effectively stripping a significant amount of OH_g and OH_{aq} precursors such as O_3 and HO_2 from the gas phase flowing over its surface.

While following a generally linear trend (Fig. 2, blue circles), the gas phase-only signal was fairly variable from day to day. The source of the variability is not clear; it showed no correlation with the O_3 concentration (obtained from a nearby South Coast Air Quality Management District monitoring station), which ranged from 34 to 48 ppb, nor did it show a strong dependence on solar intensity (Fig. 3), or a combination of these two variables. However, the variability can be problematic for aerosol OH_{aq} measurements especially for low mass loadings or particles with low activity, for which the variability can be as large as 40 - 50% of the measured.

The orange dotted line in Fig. 3 shows the result for an ambient gas-phase only sample to which (NH₄)₂SO₄ particles were added during daytime. The resulting OH_{aq} is at the low end of the gas phase-only measurements (config. 4), suggesting that uptake into the aqueous phase of the nascent droplets within the spot sampler does not appreciably increase signal above the uptake of OH_g/OH precursors from the gas phase. In contrast to these results, Jung et al. (2010) observed appreciable uptake of H₂O₂ and NH₃ into droplets within the Virtual Aerosol Concentration Enrichment System (VACES). The VACES grows particles into droplets, but it heavily concentrates the droplets/particles by separating out the gas phase, while the Liquid Spot Sampler maintains the same ratio of particles to gas.

To remove gas phase artifacts that complicate OH_{aq} quantification, we implemented and characterized an activated carbon denuder. Figs. 2 (pink squares and green squares)

show OH_{aq} concentrations collected from the gas phase only, after addition of the activated carbon denuder (Tab. 1 config. 5). The denuder almost entirely removes the OH_{aq} signal from the gas phase; the gas phase background OH_{aq} concentrations are scattered around zero for both measurements at West Los Angeles and at the Southern Great Plains Site. Particle losses for particles below 700 nm at our flow rate of 1.5 Lpm were less than 10%. The manufacturer reports similarly small losses for larger particles.

3.2 Collection of particles too small to act as cloud condensation nuclei (CCN)

The spot sampler collects particles as small as 5nm, well below the cutoff for CCN activity in the atmosphere, which is not ideal. However, although the number concentration of these non-CCN is large, their mass contribution is small. The size at which 50% of particles activate (D_{50}) falls in the 40-150 nm range (Komppula et al., 2005; McFiggins et al., 2006; Kerminen et al., 2012) depending primarily on the particle chemical composition and water vapor supersaturation (Kerminen et al. 2012). For urban size distributions (Cabada et al. 2004, Chen et al. 2011, Hu et al. 2012) and a mid-range D_{50} of 100 nm, the contribution to $PM_{2.5}$ of non-CCN would be about 3%, with a range of 1-5% depending on the particle size distribution. The lower and upper limits, corresponding to D_{50} s of 40 and 150 nm, are about 1% and 5%, respectively, with a range of 0.3-12%. The contributions of non-CCN to TSP will be smaller. While the OH burst depends on chemical composition, the activity of non-CCN would not likely exceed that of the CCN to such a degree that the bias would become a significant source of error.

3.3 OH formation by Particles collected on Filters.

348

349

350

351

352

353

354

355

356

357

358

359

360

361

362

363

364

365

366

367

368

Fig. 4, yellow checkered bars, show the interquartile ranges of OH burst measurements for filter samples collected in West LA for PM_{2.5}, and TSP. Values averaged $(71 \pm 59 \text{ nM} \text{ and } 102 \pm 74 \text{ nM})$ for PM_{2.5}, and TSP, respectively. The OH burst for filter samples collected during the daytime at the West LA site are consistently several times lower than daytime samples observed previously, in Claremont, CA during summer (320 ± 130 nM) (Kuang et al. 2020) and in Fresno, CA (430 ± 280 nM) (Paulson et al. 2019); Fresno nighttime samples were even higher. While the reason for this is not yet understood, the three sites are characterized by different sources of particulate matter. The west Los Angeles site is usually impacted by mostly fresh primary or very aged mixed aerosols due to its location near the coast and edge of the conurbation, while the Claremont site (located about 80 km inland) during this sampling period (late summer) experiences high levels of secondary aerosols and a mix of fresh and moderately aged primary aerosols (Wang 2012, Kuang et al. 2020). The Fresno, CA measurements were made during January and February, a period characterized by large contributions from biomass burning from residential woodburning as well as mixed aerosols of mixed urban and agricultural origin (Paulson et al. 2019).

3.3.1 Slow Formation of OH_{aq} in the Filter Extracts and DtR Collection Liquid.

Table S1 shows detailed sampling parameters and OH_{aq} formation quantities and rates. The filter extracts exhibited an OH burst followed by a variable OH formation slow phase, which is generally linear (see Paulson et al. 2019). The slow phase had a median value of

o.45 nM min⁻¹ and a range from o.21 – 2.5 nM min⁻¹, normalized to an aerosol:liquid v:v dilution ratio of 25,000. To correct for slow-phase OH_{aq} formation in the DtR collection solution, we subtracted the slow phase formation measured for the parallel filters for a time equal to half of the DtR collection time. This correction accounted for 25 ± 8 and 16 ± 10 % of the total DtR signal.

0

3.4 DtR Measurements

3.4.1 DtR Limit of Detection

For the configuration with the gas denuder, the Spot Sampler-based DtR method can measure the OH_{aq} burst for around 1 µg of aerosols with low reactivity. For ambient sampling with the addition of an activated charcoal denuder, the gas phase background is negligible. Other sources of error, which include the calibration, the blank and the slow phase correction result in a method uncertainty of about 10 nM OH. The low end of OH production is around 35 nM/µg in the collection liquid. Further, our tests have shown that the hTA fluorophore formed upon reaction of TA and OH_{aq} is stable over tens of hours at room temperature. Therefore, longer sampling times can be implemented with negligible loss of the fluorescent hTa, allowing robust OH quantification over long sampling periods if needed.

387 3.4.2 Measurements in West Los Angeles

The OH burst measured in the Direct-to-Reagent samples averaged 507 ± 365 nM (Figs. 4 and 5). The OH burst was substantially higher in the DtR samples compared to filter samples for both PM size ranges (Figs 4 and 5); the ratio of DtR to filter samples was 5.85 ± 2.85 , and 6.27 ± 2.24 for ambient PM_{2.5}, and TSP respectively (Figure S₃). There are no published DtR measurements of OH formation by particles for comparison.. Fig. 5 shows the relationship between the filter and DtR parallel samples. The dataset is modest but it suggests that the two measures are reasonably strongly correlated.

4. Discussion

DtR and Filter Measurement Comparison.

There are multiple possible sources of particle-associated OH_{aq} formation, including: (i) OH present in the particles; (ii) reactions of labile particle-derived species leading to OH_{aq} production, such as the reactions of superoxide (O_2^-) and the hydroperoxyl radical (HO_2) or alkylperoxy radicals with H_2O_2 (De Laat and Le 2005, Wang 2012); (iii) labile species such as organic hydroperoxides which decay to produce OH (Tong et al. 2016); and (iv), fast reactions of species such as peracetic acid with Fe(II); peracetic acid has been shown to react rapidly with Fe(II) to produce OH (Paulson et al. 2019).

While some species may decay very rapidly, filter collection requires hours, so even relatively long-lived species may decay before being detected (Zhang et al. 2022). Zhou et al. (2018) reported that a significant fraction (\sim 60 \pm 20 %) of ROS is highly reactive and prone to decay during PM filter sampling prior to toxicological analysis. Fuller et al. (2014)

observed a decrease by about a factor of five in ROS content of laboratory generated

oxidized organic aerosols within the first 15 minutes of their being capturing on PTFE filters. Recently, Brown et al. (2020) estimated up to 71% short-lived (defined as having a half-live of 5 mins or less) ROS to total hourly averaged PM-bound ROS at a site in the in Heshan, China. Zhang et al. (2022) showed that on average more than 90% of ROS in a photochemically aged mixture of primary combustion soot particles and naphthalene or βpinene aerosols were short-lived. In addition, Utinger et al. (2023) demonstrated the rapid decay of oxidizing components of (α-pinene) secondary organic aerosol using a direct-toreagent approach similar to that used here but with an ascorbic acid based assay, with simultaneous comparison to filter samples analyzed immediately after particle collection. The decay of particle-associated oxidizing species appears to occur in three phases, with one rapid ($t_{1/2} < 1 \text{ min}$), one medium decay phase ($t_{1/2} \sim 20 \text{ hrs.}$) one long-lived ($t_{1/2} \sim 1 \text{ week}$) decay phase, where the first rapid phase leads to a decrease in oxidizing activity by about ~ 75% within minutes. After a week of filter storage, ~90% of species contributing to the oxidative capacity of the particles on the filter were lost compared to a direct-to-reagent approach. Consequently, the observed lower OH formation in the extracted filter samples could be attributed to the loss of short-lived ROS and labile OH precursors. Our measurements indicate that the filters retained an average of about 15%, with a range of about 5 – 25% of the activity compared with the DtR measurements, suggesting decay in the 80 – 90% range. This is generally consistent but on the lower end of the observations for other labile species described above.

409

410

411

412

413

414

415

416

417

418

419

420

421

422

423

424

425

426

427

429 Conclusions

430

431

432

433

434

435

436

437

438

439

440

441

442

443

444

445

446

447

448

This study presents the development, characterization, and first field deployment of a novel method to accurately quantify OH production by ambient particulate matter in simulated cloud droplets using a direct-to-reagent (DtR) sampling approach. We efficiently remove gas phase measurement artefacts by implementing an activated charcoal denuder, reducing the inherent variability and background signal of the method, thus improving the method detection limit, and allowing longer sampling times. These key method developments facilitate particle-derived OH measurements even under low-pollution conditions, with lower particle concentrations and potentially particles with lower OH activity. In addition, we show that whilst traditional filter-based methods provide some detail regarding particle-derived OH formation, our direct-to-OH approach captures the full extent of the OH burst compared to filters. The ratio of DtR:filter OH measurements are variable, where we observed 3 - 9 times more OH produced in the DtR method compared to filter-based measurements. We attribute this to loss of OH activity of the particles on filters. This demonstrates the need for direct-to-reagent methods to capture highly reactive components of ambient particulate matter, providing more robust and accurate measurements of OH_{aq} produced from ambient particulate matter. Accurate OH measurements are essential to fully determine the role of particle-derived OH_{aq} in cloud droplets, developing our understanding of the role OH_{aq} plays in atmospheric chemistry and cloud processing.

450 Acknowledgements

- This material is based upon work supported by the National Science Foundation under Grant No.
- 452 ATM2001187, and by the Department of Energy under Award no. DE-SC0022159.

References

- Arakaki, T. and B. C. Faust (1998). "Sources, sinks, and mechanisms of hydroxyl radical (•OH) photoproduction and consumption in authentic acidic continental cloud waters from Whiteface Mountain, New York: The role of the Fe(r) (r = II, III) photochemical cycle." <u>Journal of Geophysical Research: Atmospheres</u> **103**(D3): 3487-3504.DOI: 10.1029/97JD02795.
- Bardouki, H., M. B. da Rosa, N. Mihalopoulos, W. U. Palm and C. Zetzsch (2002). "Kinetics and mechanism of the oxidation of dimethylsulfoxide (DMSO) and methanesulfinate (MSI–) by OH radicals in aqueous medium." <u>Atmospheric Environment</u> **36**(29): 4627-4634.DOI: https://doi.org/10.1016/S1352-2310(02)00460-0.
 - Bates, J. T., T. Fang, V. Verma, L. Zeng, R. J. Weber, P. E. Tolbert, J. Y. Abrams, S. E. Sarnat, M. Klein, J. A. Mulholland and A. G. Russell (2019). "Review of Acellular Assays of Ambient Particulate Matter Oxidative Potential: Methods and Relationships with Composition, Sources, and Health Effects." <u>Environmental Science & Technology</u> **53**(8): 4003-4019.DOI: 10.1021/acs.est.8b03430.
 - Bianco, A., M. Passananti, H. Perroux, G. Voyard, C. Mouchel-Vallon, N. Chaumerliac, G. Mailhot, L. Deguillaume and M. Brigante (2015). "A better understanding of hydroxyl radical photochemical sources in cloud waters collected at the puy de Dôme station experimental versus modelled formation rates." <u>Atmos. Chem. Phys.</u> **15**(16): 9191-9202.DOI: 10.5194/acp-15-9191-2015.
 - Bianco, A., M. Vaïtilingom, M. Bridoux, N. Chaumerliac, J.-M. Pichon, J.-L. Piro and L. Deguillaume (2017). "Trace Metals in Cloud Water Sampled at the Puy De Dôme Station." Atmosphere 8(11): 225.
 - Brown, R. A., S. Stevanovic, S. Bottle, H. Wang, Z. Hu, C. Wu, B. Wang and Z. Ristovski (2020). "Relationship between Atmospheric PM-Bound Reactive Oxygen Species, Their Half-Lives, and Regulated Pollutants: Investigation and Preliminary Model." <u>Environmental Science & Technology</u> **54**(8): 4995-5002.DOI: 10.1021/acs.est.9b06643.
- Cabada, J. C., S. Rees, S. Takahama, A. Khlystov, S. N. Pandis, C. I. Davidson and A. L. Robinson (2004). "Mass size distributions and size resolved chemical composition of fine particulate matter at the Pittsburgh supersite." <u>Atmospheric Environment</u> **38**(20): 3127-3141.
- Campbell, S. J., S. Stevanovic, B. Miljevic, S. E. Bottle, Z. Ristovski and M. Kalberer (2019).

 "Quantification of Particle-Bound Organic Radicals in Secondary Organic Aerosol."

 Environmental Science & Technology 53(12): 6729-6737.DOI: 10.1021/acs.est.9b00825.

- Chen, S.-C., C.-J. Tsai, H.-D. Chen, C.-Y. Huang and G.-D. Roam (2011). "The influence of relative humidity on nanoparticle concentration and particle mass distribution measurements by the MOUDI." Aerosol Science and Technology 45(5): 596-603.
- De Laat, J. and T. G. Le (2005). "Kinetics and modeling of the Fe (III)/H2O2 system in the presence of sulfate in acidic aqueous solutions." <u>Environ. Sci. Technol.</u> **39**(6): 1811-1818.
- Deguillaume, L., M. Leriche, K. Desboeufs, G. Mailhot, C. George and N. Chaumerliac (2005).

 "Transition metals in atmospheric liquid phases: Sources, reactivity, and sensitive parameters."

 Chem. Rev. 105(9): 3388-3431.
 - Eiguren-Fernandez, A., N. Kreisberg and S. Hering (2017). "An online monitor of the oxidative capacity of aerosols (o-MOCA)." <u>Atmos. Meas. Tech.</u> **10**(2): 633-644.DOI: 10.5194/amt-10-633-2017.
 - El-Sayed, M. M. H., Y. Wang and C. J. Hennigan (2015). "Direct atmospheric evidence for the irreversible formation of aqueous secondary organic aerosol." <u>Geophysical Research Letters</u> **42**(13): 5577-5586.DOI: https://doi.org/10.1002/2015GL064556.
 - Ervens, B. (2018). Progress and Problems in Modeling Chemical Processing in Cloud Droplets and Wet Aerosol Particles. <u>Multiphase Environmental Chemistry in the Atmosphere</u>, American Chemical Society. **1299:** 327-345.
 - Ervens, B., A. Sorooshian, Y. B. Lim and B. J. Turpin (2014). "Key parameters controlling OH-initiated formation of secondary organic aerosol in the aqueous phase (aqSOA)." <u>Journal of Geophysical Research: Atmospheres</u> **119**(7): 3997-4016.DOI: https://doi.org/10.1002/2013JD021021.
 - Fuller, S. J., F. P. H. Wragg, J. Nutter and M. Kalberer (2014). "Comparison of on-line and off-line methods to quantify reactive oxygen species (ROS) in atmospheric aerosols." <u>Atmospheric Environment</u> 92: 97-103.DOI: http://dx.doi.org/10.1016/j.atmosenv.2014.04.006.
 - Fung, K. M., C. L. Heald, J. H. Kroll, S. Wang, D. S. Jo, A. Gettelman, Z. Lu, X. Liu, R. A. Zaveri, E. C. Apel, D. R. Blake, J. L. Jimenez, P. Campuzano-Jost, P. R. Veres, T. S. Bates, J. E. Shilling and M. Zawadowicz (2022). "Exploring dimethyl sulfide (DMS) oxidation and implications for global aerosol radiative forcing." <u>Atmos. Chem. Phys.</u> 22(2): 1549-1573.DOI: 10.5194/acp-22-1549-2022.
 - Gonzalez, D. H., X. M. Kuang, J. A. Scott, G. O. Rocha and S. E. Paulson (2018). "Terephthalate probe for hydroxyl radicals: yield of 2-hydroxyterephthalic acid and transition metal interference." Analytical Lett. **51**(15): 2488-2497.DOI: 10.1080/00032719.2018.1431246.
- Griffith, S. M., R. F. Hansen, S. Dusanter, V. Michoud, J. B. Gilman, W. C. Kuster, P. R. Veres, M. Graus, J. A. de Gouw, J. Roberts, C. Young, R. Washenfelder, S. S. Brown, R. Thalman, E. Waxman, R. Volkamer, C. Tsai, J. Stutz, J. H. Flynn, N. Grossberg, B. Lefer, S. L. Alvarez, B. Rappenglueck, L. H. Mielke, H. D. Osthoff and P. S. Stevens (2016). "Measurements of hydroxyl and hydroperoxy radicals during CalNex-LA: Model comparisons and radical budgets." Journal of Geophysical Research: Atmospheres 121(8): 4211-4232.DOI: https://doi.org/10.1002/2015JD024358.
- Hanson, D. R., J. B. Burkholder, C. J. Howard and A. R. Ravishankara (1992). "Measurement of hydroxyl and hydroperoxy radical uptake coefficients on water and sulfuric acid surfaces." <u>The</u> Journal of Physical Chemistry **96**(12): 4979-4985.DOI: 10.1021/j100191a046.
- Hasheminassab, S., P. Pakbin, R. J. Delfino, J. J. Schauer and C. Sioutas (2014). "Diurnal and seasonal trends in the apparent density of ambient fine and coarse particles in Los Angeles."

 Environ Pollut 187: 1-9.DOI: 10.1016/j.envpol.2013.12.015.

- Hecobian, A., A. Evanoski-Cole, A. Eiguren-Fernandez, A. P. Sullivan, G. S. Lewis, S. V. Hering and J. L. Collett Jr (2016). "Evaluation of the Sequential Spot Sampler (S3) for time-resolved measurement of PM2.5 sulfate and nitrate through lab and field measurements." <u>Atmos. Meas.</u> <u>Tech.</u> 9(2): 525-533.DOI: 10.5194/amt-9-525-2016.
- Hering, S. V., S. R. Spielman and G. S. Lewis (2014). "Moderated, Water-Based, Condensational Particle Growth in a Laminar Flow." <u>Aerosol Science and Technology</u> **48**(4): 401-408.DOI: 10.1080/02786826.2014.881460.
- Hoffmann, E. H., A. Tilgner, R. Schrödner, P. Bräuer, R. Wolke and H. Herrmann (2016). "An advanced modeling study on the impacts and atmospheric implications of multiphase dimethyl sulfide chemistry." Proc. Nat'l. Acad. Sci. 113(42): 11776-11781.DOI: 10.1073/pnas.1606320113.
 - Hu, M., J. Peng, K. Sun, D. Yue, S. Guo, A. Wiedensohler and Z. Wu (2012). "Estimation of size-resolved ambient particle density based on the measurement of aerosol number, mass, and chemical size distributions in the winter in Beijing." <u>Environmental science & technology</u> **46**(18): 9941-9947.
 - Jung, H., C. Arellanes, Y. Zhao, S. Paulson, C. Anastasio and A. Wexler (2010). "Impact of the Versatile Aerosol Concentration Enrichment System (VACES) on Gas Phase Species." Aerosol Science and Technology 44(12): 1113-1121.DOI: 10.1080/02786826.2010.512028.
 - Kaur, R. and C. Anastasio (2017). "Light absorption and the photoformation of hydroxyl radical and singlet oxygen in fog waters." <u>Atmos. Env.</u> **164**: 387-397.DOI: https://doi.org/10.1016/j.atmosenv.2017.06.006.
 - Kerminen, V. M., M. Paramonov, T. Anttila, I. Riipinen, C. Fountoukis, H. Korhonen, E. Asmi, L. Laakso, H. Lihavainen, E. Swietlicki, B. Svenningsson, A. Asmi, S. N. Pandis, M. Kulmala and T. Petäjä (2012). "Cloud condensation nuclei production associated with atmospheric nucleation: a synthesis based on existing literature and new results." <u>Atmos. Chem. Phys.</u> 12(24): 12037-12059.DOI: 10.5194/acp-12-12037-2012.
 - Kuang, X. M., G. D.H., J. A. Scott, K. K. T. Vu, A. S. Hasson, T. Charbouillot, L. Hawkins and S. E. Paulson (2020). "Cloud Water Chemistry associated with Urban Aerosols: Hydroxyl Radical Formation, Soluble Metals, Fe(II), Fe(III) and Quinones." <u>Earth & Space Chem.</u> DOI: https://doi.org/10.1021/acsearthspacechem.9b00243.
 - Kuang, X. M., J. A. Scott, G. O. da Rocha, R. Betha, D. J. Price, L. M. Russell, D. R. Cocker and S. E. Paulson (2017). "Hydroxyl radical formation and soluble trace metal content in particulate matter from renewable diesel and ultra low sulfur diesel in at-sea operations of a research vessel." Aer. Sci. Tech. **51**(2): 147-158.DOI: 10.1080/02786826.2016.1271938.
 - Kunihisa, R., A. Iwata, M. Gen, C. K. Chan and A. Matsuki (2020). "Application of SERS on the chemical speciation of individual Aitken mode particles after condensational growth." <u>Aerosol Science and Technology</u> **54**(7): 826-836.DOI: 10.1080/02786826.2020.1730298.
- Luo, X., X. Yang, X. Qiao, Y. Wang, J. Chen, X. Wei and W. J. G. M. Peijnenburg (2017).

 "Development of a QSAR model for predicting aqueous reaction rate constants of organic chemicals with hydroxyl radicals." <u>Environmental Science: Processes & Impacts</u> 19(3): 350-356.DOI: 10.1039/C6EM00707D.
- Misra, C., M. Singh, S. Shen, C. Sioutas and P. M. Hall (2002). "Development and evaluation of a personal cascade impactor sampler (PCIS)." <u>Journal of Aerosol Science</u> **33**(7): 1027-1047.DOI: https://doi.org/10.1016/S0021-8502(02)00055-1.

- Nguyen, T. B., M. M. Coggon, R. C. Flagan and J. H. Seinfeld (2013). "Reactive Uptake and Photo-Fenton Oxidation of Glycolaldehyde in Aerosol Liquid Water." <u>Environmental Science</u> & Technology 47(9): 4307-4316.DOI: 10.1021/es400538j.
- Paulson, S. E., P. J. Gallimore, X. M. Kuang, J. R. Chen, M. Kalberer and D. H. Gonzalez (2019).

 "A light-driven burst of hydroxyl radicals dominates oxidation chemistry in newly activated cloud droplets." Science Advances 5(5): eaav7689.DOI: 10.1126/sciadv.aav7689.
 - Sareen, N., A. G. Carlton, J. D. Surratt, A. Gold, B. Lee, F. D. Lopez-Hilfiker, C. Mohr, J. A. Thornton, Z. Zhang, Y. B. Lim and B. J. Turpin (2016). "Identifying precursors and aqueous organic aerosol formation pathways during the SOAS campaign." <u>Atmos. Chem. Phys.</u> **16**(22): 14409-14420.DOI: 10.5194/acp-16-14409-2016.
 - Sehested, K., J. Holcman and E. J. Hart (1983). "Rate constants and products of the reactions of eaq, dioxide(1-) (O2-) and proton with ozone in aqueous solutions." <u>The Journal of Physical Chemistry</u> **87**(11): 1951-1954.DOI: 10.1021/j100234a024.
 - Taghvaee, S., A. Mousavi, M. H. Sowlat and C. Sioutas (2019). "Development of a novel aerosol generation system for conducting inhalation exposures to ambient particulate matter (PM)."

 <u>Science of The Total Environment</u> 665: 1035-1045.DOI: https://doi.org/10.1016/j.scitotenv.2019.02.214.
 - Tong, H., A. M. Arangio, P. S. J. Lakey, T. Berkemeier, F. Liu, C. J. Kampf, W. H. Brune, U. Pöschl and M. Shiraiwa (2016). "Hydroxyl radicals from secondary organic aerosol decomposition in water." <u>Atmos. Chem. Phys.</u> **16**(3): 1761-1771.DOI: 10.5194/acp-16-1761-2016.
 - Utinger, B., S. J. Campbell, N. Bukowiecki, A. Barth, B. Gfeller, R. Freshwater, H. R. Ruegg and M. Kalberer (2023). "An Automated Online Field Instrument to Quantify the Oxidative Potential of Aerosol Particles via Ascorbic Acid Oxidation." <u>Atmos. Meas. Tech. Discuss.</u> **2023**: 1-20.DOI: 10.5194/amt-2023-14.
 - Wang, S., Y. Zhao, A. W. H. Chan, M. Yao, Z. Chen and J. P. D. Abbatt (2023). "Organic Peroxides in Aerosol: Key Reactive Intermediates for Multiphase Processes in the Atmosphere." <u>Chemical Reviews</u> **123**(4): 1635-1679.DOI: 10.1021/acs.chemrev.2c00430.
 - Wang, Y., C. Arellanes, C. and S.E. Paulson (2012). "Hydrogen Peroxide Associated with Ambient Fine Mode, Diesel and Biodiesel Aerosol Particles in Southern California. "Aerosol Sci.& Technol. 10.DOI: 10.1080/02786826.2011.633582.
 - Yang, Y., H. Wang, S. J. Smith, R. Easter, P. L. Ma, Y. Qian, H. Yu, C. Li and P. J. Rasch (2017). "Global source attribution of sulfate concentration and direct and indirect radiative forcing." Atmos. Chem. Phys. **17**(14): 8903-8922.DOI: 10.5194/acp-17-8903-2017.
 - Yu, L., J. Smith, A. Laskin, K. M. George, C. Anastasio, J. Laskin, A. M. Dillner and Q. Zhang (2016). "Molecular transformations of phenolic SOA during photochemical aging in the aqueous phase: competition among oligomerization, functionalization, and fragmentation." https://doi.org/10.1016/journal.com/ 16(7): 4511-4527.DOI: 10.5194/acp-16-4511-2016.
- Zellner, R., M. Exner and H. Herrmann (1990). "Absolute OH quantum yields in the laser photolysis of nitrate, nitrite and dissolved H2O2 at 308 and 351 nm in the temperature range 278–353 K." J. Atmos. Chem. **10**(4): 411-425.DOI: 10.1007/bf00115783.
- Zepp, R. G., B. C. Faust and J. Hoigne (1992). "Hydroxyl radical formation in aqueous reactions (pH 3-8) of iron(II) with hydrogen peroxide: the photo-Fenton reaction." Env. Sci. Tech. 26(2): 313-319.DOI: 10.1021/es00026a011.
- Zhang, Z. H., E. Hartner, B. Utinger, B. Gfeller, A. Paul, M. Sklorz, H. Czech, B. X. Yang, X. Y.
 Su, G. Jakobi, J. Orasche, J. Schnelle-Kreis, S. Jeong, T. Gröger, M. Pardo, T. Hohaus, T.

Adam, A. Kiendler-Scharr, Y. Rudich, R. Zimmermann and M. Kalberer (2022). "Are reactive oxygen species (ROS) a suitable metric to predict toxicity of carbonaceous aerosol particles?" Atmos. Chem. Phys. 22(3): 1793-1809.DOI: 10.5194/acp-22-1793-2022. Zhou, J., E. A. Bruns, P. Zotter, G. Stefenelli, A. S. H. Prévôt, U. Baltensperger, I. El-Haddad and J. Dommen (2018). "Development, characterization and first deployment of an improved online reactive oxygen species analyzer." Atmos. Meas. Tech. 11(1): 65-80.DOI: 10.5194/amt-11-65-2018.

Table 1. OH uptake/source test configurations.

Con fig.	Air	Particle type	Sample type	Setup description (see SI Blank	
	source			schematics)	
1	OH free air	None	Aerosol-to-Reagent collector background.	Compressed air $(76.5 - 80.5\% N_2 \text{ and } 19.5-23.5\% O_2)$ from a cylinder introduced at 1.5 LPM into the instrument (Fig. SI S1 (a)).	TA solution
2	OH free air	(NH ₄) ₂ SO ₄	Instrument background with (NH ₄) ₂ SO ₄ particles.	$(NH_4)_2SO_4$ solution nebulized with compressed air; (Fig. SI $S1(b)$).	TA solution
3	PM-filtered ambient air	None	Uptake of OH _g from ambient air flowing over the surface of the collection solution.	Ambient air was flowed through a HEPA-vent filter upstream of the spot sampler (Fig. SI Sı(c)).	TA solution
4	PM-filtered ambient air	(NH ₄) ₂ SO ₄	Combined uptake of OH _g in droplets grown from (NH ₄) ₂ SO ₄ particles and to surface of the collection solution.	PM-filtered ambient air used to nebulize $(NH_4)_2SO_4$ (Fig. SI $S_1(d)$).	TA solution
5	PM- filtered, gas denuded ambient air	None	Ambient air background.	A HEPA-vent filter and a gas denuder were placed upstream of the spot sampler (Fig. SI S1(e)).	TA solution
6	Ambient air	TSP, PM _{2.5}	Sampling configuration prior to addition of denuder.	For TSP, ambient air was drawn directly into the instrument. For PM _{2.5} , PCIS with 7.5 LPM bypass flow was added to the inlet to achieve the nominal flowrate of the PCIS (Fig. 1).	Config.
7	Ambient air with OH and OH precursors removed	TSP, PM _{2.5}	Standard sampling configuration.	A PCIS was used to exclude particles larger than 2.5 µm, or (for TSP) all particles were collected. A 7.5 LPM bypass flow was added to the inlet. After the PCIS, air flows through an activated carbon denuder (Fig. 1).	Config. 5

Sample Ambient aerosols Inlet Wick 9 LPM Water reservoir Portable pump **PCIS** Cold Conditioner 7.5 LPM 5°c Cold wet wall Initiator Denuder | Warm Droplet 35°c activation region 1.5 LPM • Cool • **Moderator** 12°c **Excess water** • removal region Growth tube •• **Liquid collection** of airborne • particles Spot Sampler unit

Figure 1. Left panel: Schematic of the growth tube in Spot Sampler. **Right Panel:** Final experimental schematic of the sampling setup with particle size selective inlets for the collection of PM_{2.5} and including the gas phase denuder. Most data shown here are for samples that did not include the denuder.

639 640

641642

643 644

645

646

647

648

649

650

651

652

653

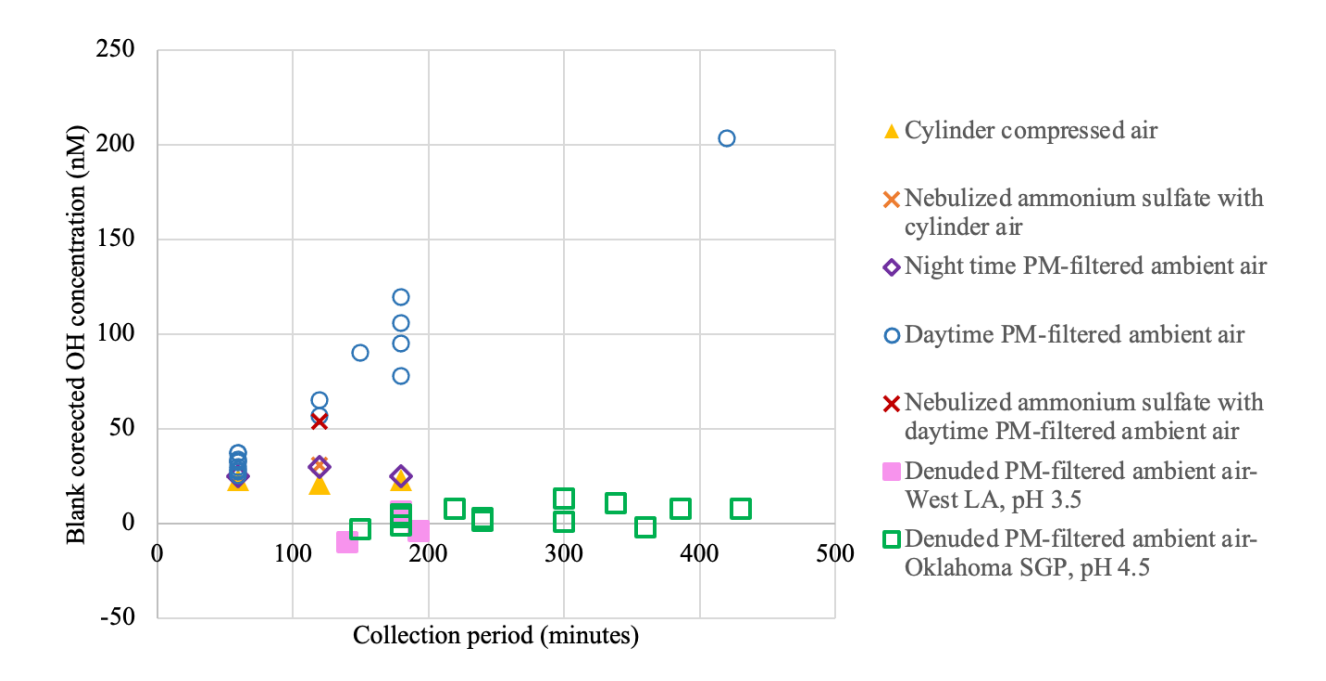


Figure 2. OH concentration associated with spot sampler collection in the absence of ambient particles of: (i) cylinder compressed air; (ii) cylinder air with aerosolized (NH₄)₂SO₄; ambient gas phase only collected during nighttime (iii); and daytime (iv); (v) daytime ambient gas phase with aerosolized (NH₄)₂SO₄ aerosols and (vi) denuded PM-filtered ambient air, for different sampling locations. All data are blank corrected.

66o

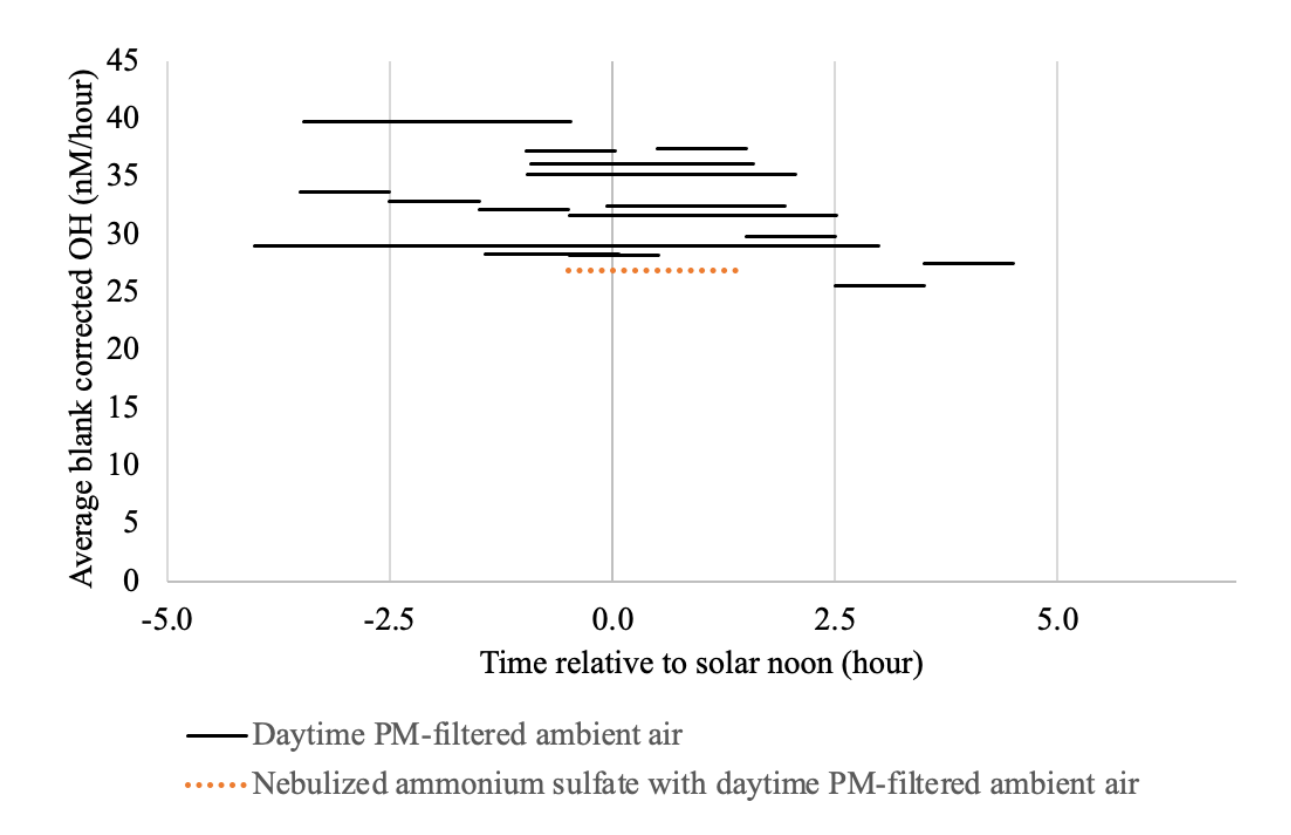


Figure 3. OH collected from gas-phase only ambient air in the collection solution vs. time of day. Since each collection event results in only one measurement, data are plotted as horizontal lines spanning the period over which the sample was collected. Black lines indicate direct sampling into the Spot Sampler. The orange dashed line represents a gas phase sample (un-denuded) with added aerosolized (NH₄)₂SO₄. All data are blank corrected.

68o



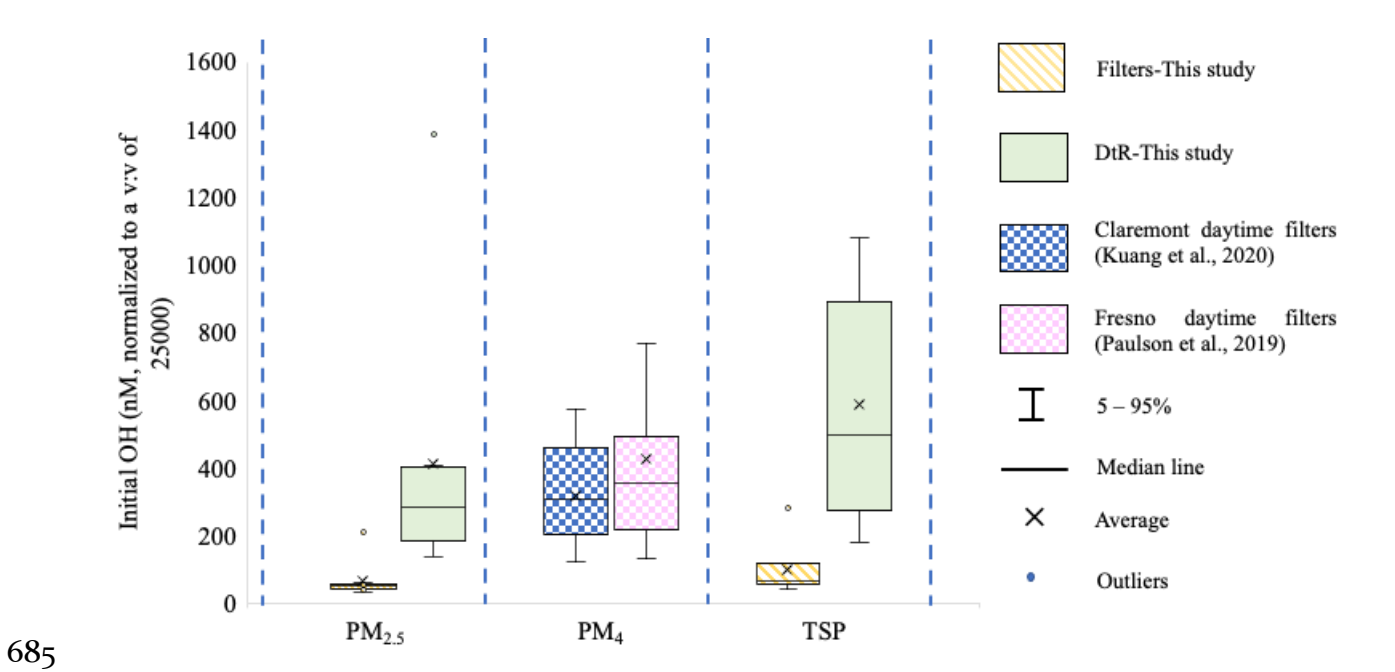


Figure 4. Interquartile plot showing the OH burst for filter samples in this study (yellow checked bars) collected in west Los Angeles, in Claremont (blue checked bar, (Kuang et al. 2020)), and in Fresno (pink checked bar, (Paulson et al. 2019)), and with Direct-to-Reagent collection (green bars) for difference particle size cuts.

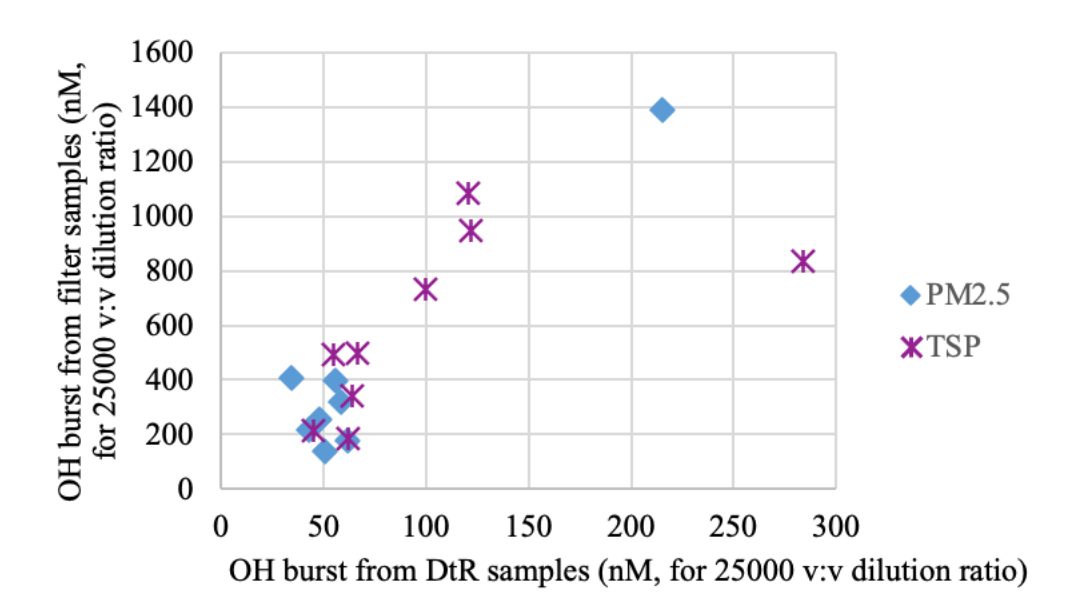


Figure 5. Scatter plot for OH burst measured from filter and DtR samples for both PM_{2.5}and TSP.